Vortex Tracking and Tropical Cyclone Genesis Factors in Simulations of Late Quaternary Paleoclimates

Ryan A. Zamora*, Robert L. Korty
Texas A&M University, College Station, Texas

1. INTRODUCTION

The ways tropical cyclones respond and adapt to changes in large-scale climate are significant and potentially consequential questions for the coming century. Analyses of simulations prepared for the 3rd Climate Model Intercomparison Project (CMIP3) showed that while environments may become more favorable for stronger storms by the end of this century, the overall number of storms may decline, largely owing to a reduction in the frequency of weak systems (e.g., Emanuel et al. 2008; Knutson et al. 2010). Newer simulations completed for CMIP5 have shown some qualitatively similar behavior, but many of the differences between late 20th and 21st century output had smaller amplitudes and only marginal significances (e.g., Knutson et al. 2013). Thus despite the significant progress over the last decade, the problem remains unfinished, and complementary research avenues have the potential for novel insights.

Here we perform many of the same analyses that have been done for climate change experiments within the CMIP suite, but apply the techniques to simulations of very different climate states. The responses are potentially instructive because the same models examined for contemporary climate change have been run for paleoclimates of the Late Quaternary Period (i.e., the Last Glacial Maximum and Holocene). These periods feature climate changes that are different and large compared to those of the present century, so the ways tropical cyclones respond to them offer interesting cases to contrast with findings reported from work with CMIP models.

The Last Glacial Maximum occurred 21,000 years ago (21ka) and featured tropical surface temperatures colder by 2-3°C than the modern world. Ice sheets covered many Northern Hemisphere continents, and atmospheric concentrations of CO_2 were only 185 ppm. Korty et al. (2012a) showed that despite these changes, many of the large-scale environmental conditions necessary for tropical cyclone genesis today were similarly favorable (and in some regions even more favorable) for genesis in the colder climate. The colder ocean temperatures are bound to a colder atmosphere, and the transfer of heat between the two media can occur as efficiently as in the modern world. The changes in environmental parameters shown by Korty et al.

(2012a, b) predict responses in the climatology of tropical cyclones, but comparisons with actual model generated storms or downscaled events has yet to be done. That is the purpose of this work, and the comparison between simulated events and the simulated large-scale environment offers a potentially useful test of the ability to extrapolate empirical genesis indices to other climates.

We analyze output from simulations of NCAR's Community Earth System Model (CESM) prepared for the most recent paleoclimate model intercomparison project (PMIP3) which were prepared concurrently with CMIP5. The advantage of this simulation is that it contains 6 hourly output for the LGM, Mid-Holocene 6ka, and Pre-Industrial Era periods at the same spatial resolution as the CMIP5 runs (~1° by 1°). This temporal output frequency is necessary to track model-generated storms, and the resolution is comparable to models others have analyzed from CMIP. The limitation of our approach is that most modeling groups archive paleoclimate output in monthly means, eliminating the possibility of tracking vortices and comparing across an ensemble of models. Nevertheless, we view this analysis of the available data as an important first step that can be compared to results from the same model's contemporary simulations.

2. VORTEX TRACKING

General circulation models produce features with tropical cyclone-like structures, which can be tracked using algorithms developed to identify their defining characteristics (e.g Vitart and Stockdale, 2001; Camargo et al. 2002). These methods track systems when specific model-dependant thermodynamic and kinematic variables exceed thresholds. Connecting nearby points that exceed one of these thresholds identifies model-generated tropical cyclone tracks. Should the track last longer than a couple days, it is deemed a tropical cyclone. For our analysis, we have adopted the Camargo et al. (2002) algorithm, which will be briefly summarized below (for a more comprehensive overview, see Camargo et al. 2002).

First, the algorithm searches for regions where the amplitude of the relative vorticity exceeds a value of positive (negative) 3.5×10^{-5} s^{-1} in the Northern (Southern) Hemisphere. Next, a matrix of grid boxes centered on the region where the threshold was exceeded is found, and iterated to the next time step (6 hours in our dataset). The algorithm again searches for an exceeded relative vorticity threshold, however only within the matrix created previously. Should a region where the threshold is exceeded be found be found

* *Corresponding author address*: Ryan A. Zamora, Texas A&M University, Dept. of Atmospheric Sciences, College Station, TX 77843-3150; e-mail: ryan.zamora@tamu.edu

again, the process is repeated and are determined to be a segment of a singular tropical cyclone track. In addition to the vorticity threshold, other thresholds must be exceeded such as the surface wind speed, temperature anomaly at three pressure levels (700, 500, and 300 hPa), and mean speed. The algorithm continues to iterate until one of these criteria is not met, and the storm is designated as complete. Upon completion of detection of all storms during the time period, an assessment of possible duplicate or piecewise storms is made. Duplicate storms are removed, while storms that are deemed to be parts of a single track, are combined. This evaluation makes the algorithm more accurate by removing bogus tropical cyclones.

Climate	Model Length	Model Storms Generated
Pre-Industrial Era	35 years	1775
Mid-Holocene	32 years	1650
Last Glacial Maximum	31 years	1344

Table 1 Vortex detection and tracking algorithm output information for three CESM climate simulations

Information on the output generated from the vortex detection and tracking algorithm is given in Table 1. The average number of model storms formed per year for the Pre-Industrial Era and Mid-Holocene simulations are quite similar (~ 51 storms/year), with lower genesis in the LGM simulation (~43 storms/year, owing mostly to the much colder climate). TCs are generated in basins qualitatively similar to climatology, with the exception of the Atlantic Ocean where CESM has a well-known bias of generating too few storms. Model resolution affects the number of features a given model will produce, with coarser runs generally yielding fewer runs than nature. Each run considered here has common resolution of ~1° by 1°.

In an effort to show the value of the tracking algorithm, a sample track is shown in Figure 1. For the sake of brevity, this track was chosen in order to showcase an example of a typical, long-lasting storm.
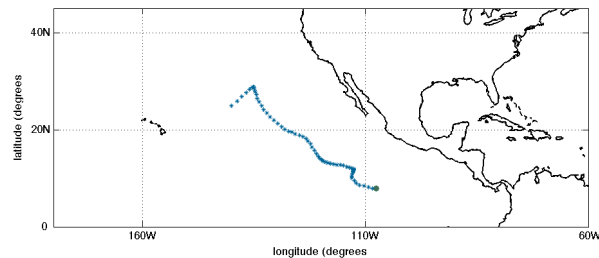

Figure 1 Sample model track generated from the vortex and tracking algorithm. The genesis location (green) and track points (blue) are denoted.

Figure 2 shows how environmental parameters vary in the sample track depicted in Figure 1. Variations in wind shear and minimum moist static energy relative to their climatological means at those locations over the

lifetime of the storm are given. The storm's change in strength can be judged by the variations in vorticity and sea level pressure. Both show an increase in strength until ~Nov. 16 and then begin to diminish in strength. While changes in strength are captured with sea level pressure, the magnitude of the pressure in this storm (along with a large number of those output from the vortex tracking algorithm) is quite high as compared to what is seen in nature. Wind shear is highly variable, with low wind shear at the beginning of the storm's lifetime (necessary for TC development), and higher values for wind shear in the latter part of its lifetime (assists in storm dissipation).
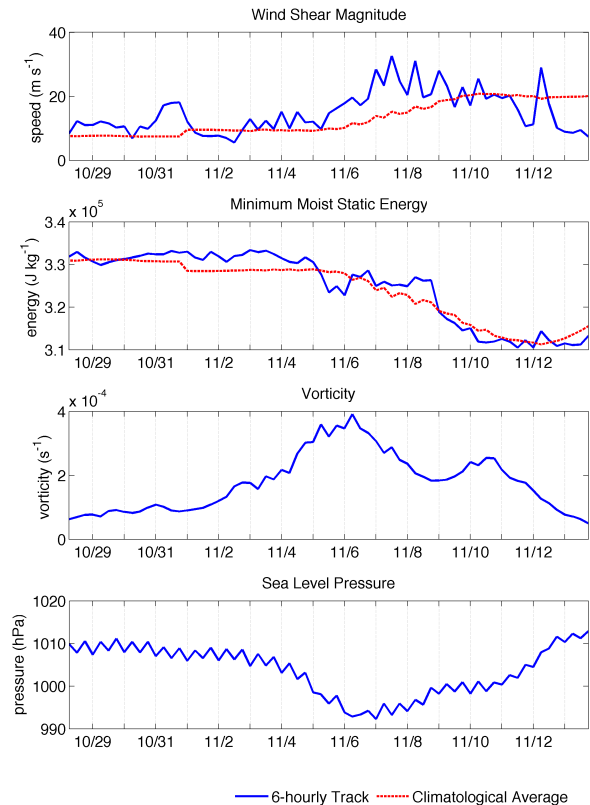

Figure 2 Environmental parameters along model generated storm track (blue) and climatological mean (red). (a) Wind shear magnitude [m/s], (b) minimum moist static energy [J/kg], (c) Vorticity [1/s], and sea level pressure [hPa].

Moist static energy is a combination of the internal, latent, and potential energies, given by:

$$h = c_p T + L_v q + gz \tag{1}$$

where c_p is the specific heat capacity at constant pressure, T is temperature, L_v is the latent heat of vaporization, q is the specific humidity, and gz is the geopotential height. Large values of h (common in the tropics) are indicative of saturated regions, and its value decreases (increases) with height from the surface (mid-troposphere). The parabolic variation of its value with

height is useful in determining how saturated the mid-troposphere is since its minimum value will reside there. Noting variations in minimum moist static energy along the storm track (Figure 2), therefore, is a guide for available moisture in the center of the storm. The amount of available moisture is largest at the beginning of the storm's lifetime and decreases steadily after Nov. 15 concurrent with decreases in both vorticity and sea level pressure. Near the end of the storm's lifetime, the minimum of h has decreased dramatically. Although this is a single case study, the environmental parameters do a fair job as predictors to changes in storm intensity.

3. TROPICAL CYCLONE GENESIS FACTORS

Potential intensity (PI) is the thermodynamic limit to the strength of tropical cyclones (TCs). To put more simply, it is the speed limit for a tropical cyclone's maximum surface wind speed. Tropical cyclones require a flux of enthalpy k (heat) from the ocean to the atmosphere, and a heated marine boundary layer parcel can then rise to its level of neutral buoyancy (LNB) based on the thermal profile that exists above it. Potential intensity is high in regions where convection can carry the heated boundary layer parcel to the tropopause, and low in regions where the sounding caps convection at shallow depths. The difference between the sea surface temperature (SST) and temperature at the level of neutral buoyancy where convection outflows (T_o) directly affects the value of PI:

$$PI = \sqrt{\frac{C_k}{C_d} \frac{SST - T_o}{T_o} \left(k_0^* - k\right)} \qquad (2)$$

Here C_k and C_d are the exchange coefficients for enthalpy and drag, respectively, k_0^* is the saturation enthalpy of the sea surface, and k is the atmospheric boundary layer enthalpy. In our analysis, we set the ratio of C_k/C_d ratio to be 0.9, which lies within the range of values tested by Emanuel (1995). Potential intensity is highest in regions of the world where thermal soundings permit deep convection, which in the present-day atmosphere correlates with regions equatorward of the 26°C isotherm. It is particularly important to note that the limiting factor is the depth of the convective layer established by the sounding, not the underlying SST; thus, in different climates (such as the LGM), the correlation between SST thresholds and high potential intensity are significantly different than in the modern world (see Korty et al. 2012a for further discussion).

Figure 3 shows the storm season mean of potential intensity (averaged JASO in Northern Hemisphere and JFMA in Southern Hemisphere). Areas able to sustain the most intense tropical cyclones are confined to places with high climatologically averaged PI. While PI provides a measure of the potential maximum surface wind speed of a TC, it can also be used to assess regions of deep convection. Korty et al. (2012a) showed the joint distribution of PI and the level of neutral buoyancy, which featured a partitioning into two major

bins: a high frequency of low PI/low-altitude LNB, and high PI/high-altitude LNB. This abrupt jump between the sets occurs roughly near the 55 m/s value for PI. Similar plots generated from the CESM dataset we examine here agree with those produced from the ensemble models (not shown). Figure # also shows the genesis locations of TC-like features followed using the vortex tracking and detection algorithm. While not strictly an index for TC genesis, the values for the climatological PI (and therefore deep convection) are highly correlated with the genesis of individual storms. Only 2% of the model storms occur at times and in regions with a PI value less than 55 m/s.
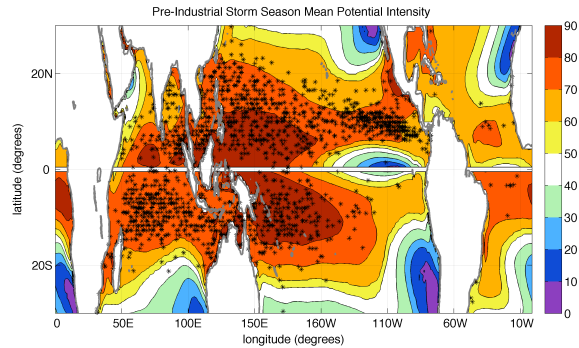

Figure 3 Storm season mean Potential Intensity (averaged JASO in Northern Hemisphere and JFMA in Southern Hemisphere) during the Pre-Industrial Era. Values shown are in m/s. Asterisks (black) denote genesis locations as derived from the vortex detection and tracking algorithm.

Both observed and modeled storms benefit from high levels of mid-tropospheric moisture (e.g. Emanuel et al. 2008; Rappin et al. 2010), which aids development by shortening the time required for moist convection to saturate the column. The ratio of moist entropy deficits to surface fluxes of enthalpy has been found to be an important non-dimensional parameter (χ) in numerical studies of genesis. The parameter is defined:

$$\chi = \frac{s_b - s_m}{s_0^* - s_b} \qquad (3)$$

where the subscripts b, m, and 0 are evaluated at the boundary layer (in our analysis taken as 925 hPa), mid-troposphere (600 hPa), and surface, respectively. The pseudo moist entropy, s, as calculated in Emanuel (1994) is defined as:

$$s = c_p \ln(T) - R_d \ln(P) + \frac{L_v q}{T} - R_v q \ln(H) \qquad (4)$$

where H is the relative humidity, q is specific humidity, and all other symbols have their common meaning. Utilizing this variable in the calculation of the mid-tropospheric moisture deficit is especially useful for our analysis of climates that differ from our own, as changes in moist entropy will scale temperature. Thus, large (small) values for χ are indicative of dry (moist) columns

of mid-tropospheric air. Figure 4 shows the storm season mean of the non-dimensional parameter, χ. A large variation in this quantity between the two storm seasons is shown, with consistently higher values (i.e. a drier mid-troposphere) in the Southern Hemisphere.
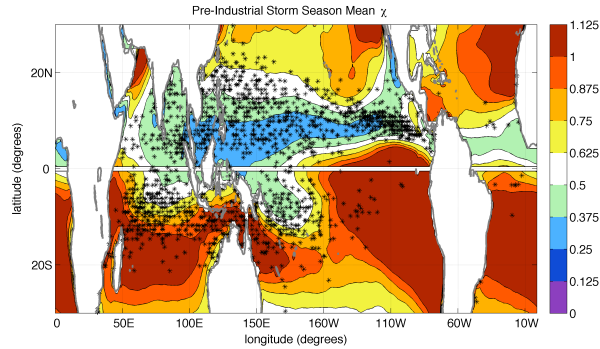

Figure 4 As in Figure 3, but for the non-dimensional parameter, χ.

During the Northern Hemisphere storm season, a majority (~64%) of the locations of TC genesis fall within values $\chi < 0.625$. Contrasting with the Southern Hemisphere storm season, a number of TCs are generated in regions of larger χ. These regions, having larger moisture deficits, would be expected to deter the formation of TCs, yet the model storms appear to be unaffected by the dry environment.

Large magnitudes for wind shear discourage TC development and intensification. Here we take the magnitude of the wind shear as the magnitude of the vector difference between 850 and 300 hPa winds (V_{shear}). While wind shear can have a relatively high sensitivity to regional and temporal variations in individual storms (as was shown in a previous section), its climatological averages are small and show little variability throughout much of the tropics, but increase in magnitude at higher latitudes.
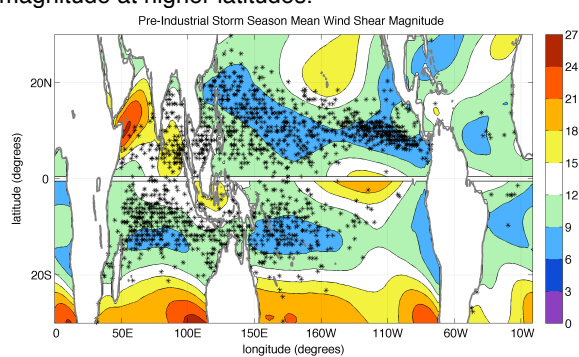

Figure 5 As in Figure 3, but for wind shear magnitude (taken as the magnitude of the vector difference between 850 and 300 hPa winds). Values shown are in m/s.

Figure 5 shows the storm season mean of the magnitude of wind shear. The majority (~87%) of genesis locations occur in regions with relatively low wind shear (< 12 m/s). The manner in where these storms are generated within low wind shear regions

follows a pattern qualitatively similar to that within high potential intensity regions in Figure 3. While high values of V_{shear} act to deter actual tropical cyclone genesis, a large number of successful genesis cases occur in regions of high wind shear in the Northern Indian Ocean.

Together, the three genesis factors discussed previously PI, χ, and V_{shear}, along with η (the absolute vorticity, which has little zonal variation but increases with latitude), make up the components of an empirically constructed genesis potential index (GPI). GPI was defined by Emanuel (2010) as:

$$GPI = \frac{a\left[\min\left(|\eta|, 4 \times 10^{-5}\right)\right]^3 \left[\max\left(MPI - 35, 0\right)\right]^2}{\chi^{4/3}\left[25 + V_{shear}\right]^4} \quad (5)$$

where a is a normalizing coefficient chosen so that the area and annual integral of GPI yields 85 storms in the present climate. This form of the index (based off of work by Emanuel (2010) and updated by Tippett et al. (2011) to clip the vorticity dependence) depicts the most favorable locations for TC genesis in the present climate. It matches the regional and seasonal cycles of observed TC genesis, but its utility in other climates is unknown.
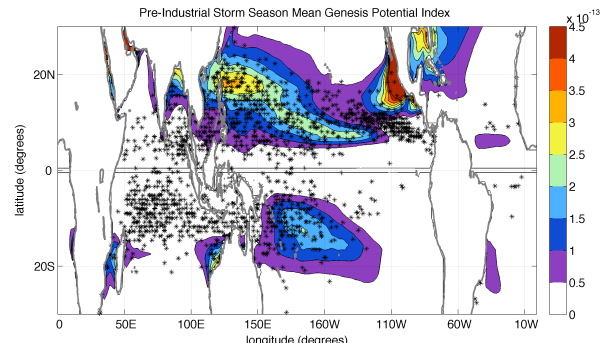

Figure 6 As in Figure 3, but for Genesis Potential Index. Values shown are in # of events m⁻² month⁻¹.

Figure 6 shows the storm season mean GPI with genesis locations from the vortex detection and tracking algorithm overlaid in black. A large number of the genesis points coincide within regions of non-negligible GPI values, especially in the Northern Hemisphere Pacific Ocean. However, the index does poorly at capturing storms in the Indian Ocean during both peak storm seasons. (CESM has a well known bias of too few storms in the Atlantic.)

These results suggest that model generated TCs are confined to regions of high potential intensity, which in the models are those with thermal profiles suitable for convection. Storms form in regions of high and low shear, as well as high and low χ within regions of high PI. The genesis index is very low in the Southern Indian Ocean owing to low magnitudes of absolute vorticity for these latitudes (not shown), but the formation of model storms is uninhibited by this background state.

4. TROPICAL CYCLOGENESIS DURING THE MID-HOLOCENE

A key goal of this research is to examine the cyclone genesis and the influence of environmental parameters on model storm development and intensification. Furthermore, however, we wish to study how model storms in different climate periods respond to environmental factors that depart significantly from their modern values.

The variations of the Earth's orbit affect the seasonal distribution of solar radiation incident at the top of the atmosphere. Precession of the Earth's equinoxes causes the closest approach to the Sun to rotate around the calendar year over an approximately 21,000-year cycle. In our current climate, this occurs during early January, but during the Mid-Holocene the perihelion occurred in mid-September (i.e. the peak of the modern Northern Hemisphere hurricane season).
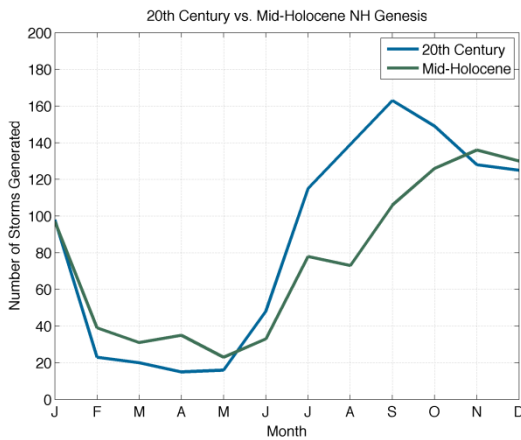

Figure 7 Seasonal tropical cyclone genesis in the Northern Hemisphere during the Pre-Industrial Era (blue) and Mid-Holocene (green) time periods. Values shown are in # of storms.

Figure 7 shows the seasonal tropical cyclone genesis of storms found using the vortex tracking and detection algorithm in the Northern Hemisphere. The sensitivity of storm genesis to the distribution of incoming solar radiation is recognized in the seasonal shift of peak hurricane season. Northern Hemisphere peak hurricane season, occurring approximately from July–October in our present climate, is shifted to September–December in the simulations of the Mid-Holocene. A delayed response in sea surface temperature (SST) to insolation causes warmer water temperatures in months later in the year than in present, while the atmosphere responds quickly to the increased radiation during summer. The ocean is relatively cool compared to the atmosphere during summer, but relatively warm during autumn, resulting in a shift in the seasonal cycle of potential intensity and other genesis factors, which mirror the shift in events generated by the general circulation model. Despite the large changes in individual months, the effects compensate between summer and fall, resulting in annual totals that are similar to those of the Pre-Industrial Era control.

Figure 8 shows the genesis factors as plotted in Figures 3–5, but for the Mid-Holocene, which depicts genesis locations occurring in a similar basin distribution as for the Pre-Industrial Era. Figure 8a shows the storm season mean PI as in Figure 3, which shows very similar results as in the Pre-Industrial Era. Likewise, values of climatological PI are highly correlated with the genesis of individual storms (<3% of the model storms occur at times and in regions with a PI value less than 55 m/s).
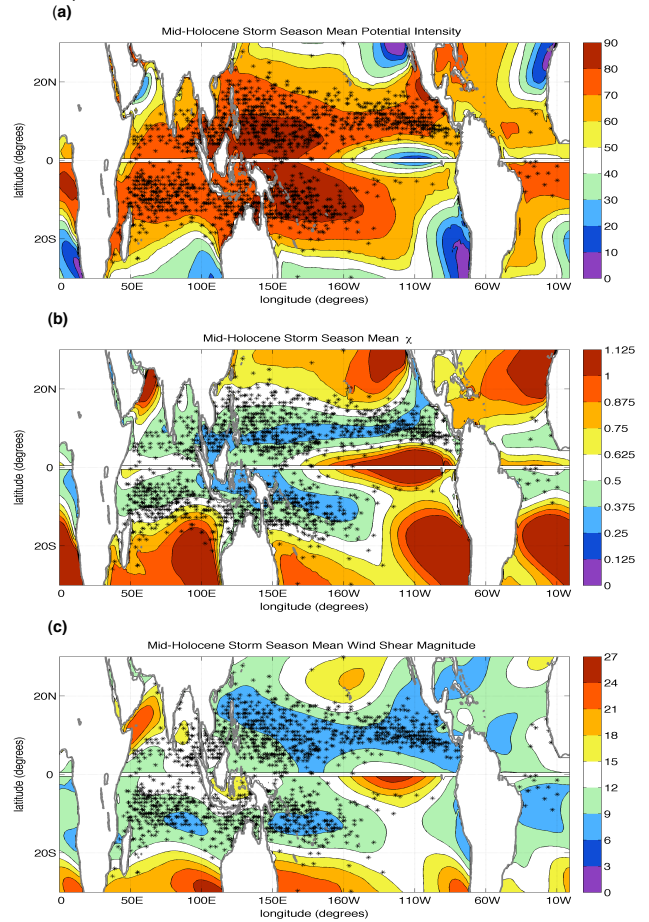

Figure 8 As in Figures 3-5, but for the Mid-Holocene.

Spatial distributions of the values for χ (Figure 8b), are quite similar as well during the Northern Hemisphere storm season, while having large variations in the Southern Hemisphere when compared with Figure 4. Values there are decreased in variety of regions (e.g. South Indian and Western South Pacific basins), which now encompass a larger amount of genesis points (76% of genesis occur in regions where $\chi < 0.625$). Wind shear (Figure 8c) as well, shows a qualitatively similar structure as the Pre-Industrial Era (Figure 5) with localized regions (e.g. Central South Pacific basin) having slightly higher values of V_{shear}. Values for $V_{shear} <$

12 m/s encompass a smaller subset of genesis locations (~81%).

5. TROPICAL CYCLOGENESIS DURING THE LAST GLACIAL MAXIMUM

Simulations of the Last Glacial Maximum provide an interesting study, as the orbital variations during that period are very similar to the present day, while global temperatures are much colder. The total number of model-generated storms under this climate simulation (Table 1) are reduced when compared with those for the Pre-Industrial and Mid-Holocene. However, the structure of the seasonal tropical cyclogenesis (not shown) is similar to that found for the Pre-Industrial simulation (Figure 7). Because the potential intensity of a tropical cyclone is dependent on profiles supportive of deep convection, as opposed to the value of *SST*, tropical cyclones are able to exist during this period despite colder *SST*. The structure of storm season mean *PI* is similar with the previously presented simulations, albeit with slightly decreased intensities in a few regions. However, <3% of the model storms occur at times and in regions with a *PI* value less than 55 m/s, as was seen for the previous 2 simulations. Storm season mean values of χ, are similar in structure but have decreased values throughout a number of regions (e.g. Central Pacific, Northern Indian, and Atlantic Oceans) when compared with the Pre-Industrial. This simulation also encompasses the most (87%) of the genesis locations within regions having values for $\chi < 0.625$. The structure of storm season mean V_{shear} is qualitatively similar to Mid-Holocene simulations, while including 88% of the genesis locations within regions having $V_{shear} < 12$ m/s.

6. CONCLUSIONS AND FUTURE WORK

We examine how environmental parameters can act as large-scale predictors of tropical cyclones in three different climate simulations by utilizing a detection and tracking vortex algorithm. The model-generated storms exhibit quasi-realistic features that respond well to changes in parameters that both inhibit and advance tropical cyclone growth. Genesis factors are useful indicators of locating regions of potential storm development. Regions of high potential intensity facilitate deep convection and storm development, even within regions having large values for χ and high wind shear.

We are in the process of relating the modeled storms with genesis factors that vary spatially and temporally with the storm track. In addition, we look to examine the relationship between the genesis factors provided (as well as γ, an index for the ventilation of the storm) with downscaled tropical cyclone climatologies. We also plan to perform a similar analysis with downscaled storms, including those generated using Emanuel's seeding technique.

8. REFERENCES
Camargo, S. J., and S. E. Zebiak, 2002: Improving the detection and tracking of tropical cyclones in atmospheric general circulation models. *Wea. Forecasting*, **17**, 1152–1162.

Emanuel, K. A., 1995: Sensitivity of tropical cyclones to surface exchange coefficients and a revised steady-state model incorporating eye dynamics. *J. Atmos. Sci.*, **52**, 3969–3976.

Emanuel, K. A., 2010: Tropical cyclone activity downscaled from NOAA-CIRES reanalysis, 1908–1958. *J. Adv. Model. Earth Syst.*, **2**, doi:10.3894/JAMES.2010.2.1.

Emanuel, K. A., R. Sundararajan, and J. Williams, 2008: Hurricanes and global warming: Results from downscaling IPCC AR4 simulations. *Bull. Amer. Metoeor. Soc.*, **89**, 347-367.

Knutson, T. R., and Coauthors, 2010: Tropical cyclones and climate change. *Nat. Geosci.,* **3**, 157-163.

Knutson, T. R., and Coauthors, 2013: Dynamical downscaling projections of twenty-first-century Atlantic hurricane activity: CMIP3 and CMIP5 model-based scenarios. *J. Climate,* **26**, 6591-6617.

Korty, R. L., S. J. Camargo, and J. Galewsky, 2012a: Tropical cyclone genesis factors in simulations of the last glacial maximum. *J. Climate*, **25**, 4348-4365.

Korty, R. L., S. J. Camargo, and J. Galewsky, 2012b: Variations in tropical cyclone genesis factors in simulations of the Holocene Epoch. *J. Climate*, **25**, 8196–8211.

Rappin, E. D., D. S. Nolan, K. A. Emanuel, 2010: Thermodynamic control of tropical cyclogenesis in environments of radiative-convective equilibrium with shear. *Q. J. R. Meteorol. Soc.*, **136**, 1954-1971.

Tippett, M. K., S. J. Camargo, and A. H. Sobel, 2011: A Poisson regression index for tropical cyclone genesis and the role of large-scale vorticity in genesis. *J. Climate*, **24**, 2335–2357.

Vitart, F., and Stockdale, T. N., 2001: Seasonal forecasting of tropical storms using coupled GCM integrations. *Mon. Wea. Rev.*, **129**, 2521–2537.